Atomic Layer Deposition of Pd Nanoparticles on TiO2 Nanotubes for Ethanol Electrooxidation: Synthesis and Electrochemical Properties

Loïc Assaud, Nicolas Brazeau, Maïssa K. S. Barr, Margrit Hanbücken, Spyridon Ntais, E. A. Baranova, Lionel Santinacci

Atomic Layer Deposition of Pd Nanoparticles on TiO_2 nanotubes for Ethanol Electrooxidation: Synthesis and Electrochemical Properties

Loïc Assaud[†,§,⊥], Nicolas Brazeau[‡,⊥], Maïssa K. S. Barr[†], Margrit Hanbücken[†], Spyridon Ntais[‡], Elena. A. Baranova[‡,] and Lionel Santinacci[†,*]*

† Aix Marseille Université, CNRS, CINaM UMR 7325, 13288, Marseille, France

‡ Department of Chemical and Biological Engineering, Center for Catalysis Research and Innovation, University of Ottawa, 161 Louis-Pasteur St., Ottawa, ON, K1N 6N5, Canada

KEYWORDS: atomic layer deposition, electrocatalysis, direct ethanol fuel cells, titanium dioxide, palladium, nanotubes, nanoparticles.

ABSTRACT. Palladium nanoparticles are grown on TiO_2 nanotubes by atomic layer deposition (ALD) and the resulting three dimensional nanostructured catalysts are studied for ethanol electrooxidation in alkaline media. The morphology, the crystal structure and the chemical composition of the Pd particles are fully characterized using scanning and transmission electron microscopies, x-ray diffraction and x-ray photoelectron spectroscopy. The characterization revealed that the deposition proceeds onto the entire surface of the TiO_2 nanotubes leading to the formation of well-defined and highly dispersed Pd nanoparticles. The electrooxidation of ethanol

on Pd clusters deposited on TiO_2 nanotubes show not only a direct correlation between the catalytic activity and the particle size but also a steep increase of the response due to the enhancement of the metal-support interaction when the crystal structure of the TiO_2 nanotubes is modified by annealing at 450°C in air.

Introduction

The hydrogen-based production of energy is attracting more and more attention especially in fuel cells technology due to the high energy density of hydrogen. However, the H_2 storage and transportation is still a challenge. The new generation of fuel cells based on the electrooxidation of alcohols such as methanol, ethanol or ethylene glycol is an interesting alternative for the production of energy.[1] Among them, methanol and ethanol are the most promising fuels, however ethanol exhibits two key advantages over methanol: it is non-toxic and renewable fuel that can be extracted from the biomass.[2]

The kinetics of the ethanol oxidation reaction (EOR) is slow in acidic media and incomplete oxidation is generally achieved over Pt-based catalysts resulting in production of acetaldehyde and acetic acid.[3] To overcome this issue, it is possible to electrooxidize ethanol in alkaline media, where oxidation kinetics is favorable and it allows the use of a cheaper Pd-based systems.[1, 4] Various strategies aimed at further improving the catalytic activity of Pd have been proposed.[1] One of them is the addition of a second noble (Ru, Au, Ir) or non-noble (Ni, Sn) metal to Pd proved to be advantageous.[1,5-8] Another approach is the use of the appropriate supporting material that can finely disperse and stabilize Pd nanoparticles as well as show better stability than conventional carbon black.[1, 5] The catalyst support can further influence strongly the activity of the metallic particles via metal-support interaction (MSI).[9-11] The catalyst support can have an

impact on the catalyst dispersion, size and morphology. Furthermore, it can modify the electronic properties of the catalyst by changing the adsorption strength of ethanol and reaction intermediates resulting in improved catalyst stability and reactivity. The carbon-based materials are widely used as a support material in fuel cells, however carbon is not stable and corrodes under reaction conditions. In order to improve the catalyst support, it can be nanostructured (e. g. carbon nanotubes[12]) or other materials such as TiO_2 can be used.[13] Titanium dioxide is known for its high stability and that in contact with platinum group metals it shows strong metal-support interaction (SMSI) for gas phase catalytic reactions.[9] Among the numerous types of titanium dioxide nanostructures, TiO_2 nanotubes (TNTs) are very interesting, because they have a large specific area and well-defined geometry. TNTs can be obtained by various methods such as deposition in templates, molecular assembly templating, hydrothermal reaction, electrospinning and anodic oxidation.[14] The later method is straightforward and offers a large control of the tube morphology. In anodic TNTs, the charge transport and collection are facilitated by the nanotubes self-alignment, because they are connected by the Ti substrate.

The coupling of Pd nanoparticles with TNTs has been reported recently. The Pd catalysts were either chemically deposited in porous TiO_2[15-16] or electrochemically deposited on anodic TNTs.[17] Atomic layer deposition (ALD) is a method of choice to grow continuous thin layers on three-dimensional substrates exhibiting a high aspect ratio.[18-20] ALD has been used to grow oxide films to support the catalysts. More recently, it has been applied to preserve the catalysts with an ultrathin metal oxide layer or to directly grow metallic nanoparticles (see, e.g., the reviews[21-23]). In the later case, ALD is particularly interesting because it provides a precise control of the growth rate and composition of the catalyst on tortuous nanostructures.[24-25] Furthermore, metallic nanoparticles deposited by ALD exhibit similar or better catalytic activities than those grown by

other techniques, such as impregnation, ion-exchange, and deposition-precipitation.[26-27] In the recent years, several works have shown the interest of using ALD to conformally grow catalytic nanoparticles onto nanostructured substrates. Pt has been deposited onto various substrates such as ZnO or TiO_2 for alcohol oxidation, oxygen reduction or photocatalysis.[25, 28-30] Pd has been less experienced but Feng et al.[31] and Rikkinen et al.[32] report the efficient deposition of this metal onto planar Al_2O_3, ZnO and porous carbon. The aim of the present study is to conformally coat TNTs with uniformly distributed Pd clusters and to assess their promising electroactivity. The Pd nanoparticles have been grown by ALD onto anodic TNTs (Pd/TNTs). The morphology, the chemical composition and the crystal structure of the metallic clusters have been investigated in details by scanning and transmission electron microscopies (SEM, TEM), x-ray photoelectron spectroscopy (XPS) and x-ray diffraction. The electroactivity of Pd/TNTs toward ethanol electrooxidation has been evaluated by cyclic voltammetry (CV) and chronoamperometry (CA) as a function of the ALD parameters and depending on the crystalline structure of the TNTs.

Experimental

Preparation of TiO_2 nanotubes

The catalyst support consists of TiO_2 nanotubes electrochemically grown from titanium foils (Advent, 95.6 % purity) in an aqueous fluoride containing acidic electrolyte (1 M NaOH + 1 M H_3PO_4 + 0.5 % HF). Ti samples were cut in square pieces (2 × 2 cm^2) then cleaned successively by sonicating in acetone, isopropanol and methanol baths for 5 min and, finally, rinsed in deionized water and dried under a nitrogen stream. The nanotubes were grown in a teflon electrochemical cell with a circular opening exposing 1.13 cm^2 of the sample to the solution. The Ti foils, a Pt mesh and a mercury/mercurous sulfate electrode (MSE, $E° = 0.64$ V vs SHE)

served as working, counter and reference electrodes, respectively. The nanotubes were grown at room temperature under an applied potential (U) of 20 V using a high voltage potentiostat (Modulab, Solartron Analytical). The duration of the anodization was 1 h in order to grow 1 μm long nanotubes. In some cases, the TNTs were annealed in air at 450°C for 2 h to modify their crystal structure.

Atomic layer deposition of Pd

The catalysts were synthesized by atomic layer deposition in a Fiji 200 reactor from Ultratech/Cambridge Nanotech. As previously reported,[33] the Pd deposition was carried out with palladium(II)hexafluoroacetylacetonate ($Pd(hfac)_2$, 98 % from Strem Chemicals) and formalin (37 % formaldehyde in water with 10-15 % of methanol from Sigma Aldrich). The Pd canister was maintained at 90°C while the temperature of the reaction chamber was set to 200°C. The ALD cycle consisted of sequential pulse, exposure and purge of Pd precursor and formalin, alternatively. The pulse, exposure and purge durations were 1:30:30 s and 3:30:30 s for $Pd(hfac)_2$ and formalin, respectively. To increase the transport of the $Pd(hfac)_2$ toward the chamber, Ar was injected for 0.25 s into the canister prior to each $Pd(hfac)_2$ pulse. The ALD of Pd was performed on both TNTs and flat Si (100) substrates in order to facilitate some characterizations. The number of ALD cycles (N) was varied in order to adjust the catalyst loading.

Characterization methods

The morphologies of TNTs as well as the supported Pd nanoparticles were characterized by scanning and transmission electron microscopies using JEOL 6320F and JEOL 7800F SEMs and a JEOL 3010 TEM. The crystal structures of the Pd clusters and TiO_2 substrate were analyzed by x-ray diffraction (XRD) using a Rigaku RU-200 rotating anode x-ray generator (operating power 40 kV/30 mA) equipped with a Xenocs Fox3D Cu 12_INF mirror and a Mar345 image plate

detector from Rayonix. X-ray photoelectron spectroscopy measurements were performed in a KRATOS Axis Ultra DLD with a Hybrid lens mode at 140 W and pass energy of 20 eV using a monochromatic Al Kα. The Pd3d and Ti2p XPS core level spectra were analyzed using a fitting routine which decomposes each spectrum into individual mixed Gaussian-Lorentzian peaks using a Shirley background subtraction over the energy range of the fit. The deconvolution of Pd3d was performed using doublets with spin orbit splitting (SOS) 5.3 eV and intensity ratio $Pd3d_{5/2}$:$Pd3d_{3/2}$ = 3/2[34] while a peak asymmetry was used in the case of the Pd3d peak attributed to the metallic state based on the work of Hufner et al.[35] The Ti2p spectra were analyzed using doublets with SOS = 5.7 eV and intensity ratio $Ti2p_{3/2}$:$Ti2p_{1/2}$ = 2/1.[36] The Binding energy (BE) was corrected using the C1s peak at 284.8 eV as an internal standard. The accuracy of measurement of the binding energy is ± 0.1 eV while that of full width at half maximum (FWHM) is ± 0.05 eV.

Electrochemical characterizations

The electrochemical characterizations of Pd/TNTs were carried out using a BioLogic potentiostat/galvanostat in 1 M KOH with and without 1 M C_2H_5OH. The reference electrode used was a Hg/HgO (MMO, $E°$ = 0.098 vs SHE) and the counter electrode was a large surface area Pt mesh. Cyclic voltammetry (CV) were recorded at a scan rate of 25 mV s^{-1} unless otherwise stated. Chronoamperograms (CA) were obtained by holding the potential at – 0.6 V vs MMO for 5 min then stepping to – 0.2 V for 1 h. The electrochemical active surface area (ECSA) was determined by the reduction of a full monolayer of PdO in 0.5 M H_2SO_4.[37] In the following, the current density is plotted either against the geometric area of the electrode (noted "GEOM") or against the ECSA.

Results and discussion

Synthesis and characterization of the catalysts

Figure 1 shows a cross-section and a top view (inset) of the nanotubes grown at $U = 20$ V for 1 h. The typical self-ordered morphology of TNTs is observed on the SEM micrographs. The tubular features (and not pores) separated by interstitial voids are uniformly distributed over the whole sample. Since an aqueous electrolyte has been used, the tube walls have a wavy aspect. The diameter of the tubes is about 70 nm, the length is approximately 1 μm and the wall thickness is in the range of 10 nm. The as-formed nanotubes are amorphous but after annealing in air for 2 h at 450°C, they are converted to the anatase crystal phase. Although their morphology remains unchanged their physical properties such as conductivity, photo-conversion efficiency or catalytic activity can be drastically modified and, in some cases, improved.[14] In a previous study, the optimal annealing parameters (temperature, duration and atmosphere) have been described.[38] In the following, the Pd deposition has always been performed on TNTs grown under similar conditions as presented in Figure 1 with or without a subsequent annealing step.

The Pd deposition process and mechanism have been already described in several reports[33, 39-40] and will not be described again here. Figure 2 presents the evolution of the Pd deposit with respect to the number of ALD cycles (N ranging from 400 to 900 cycles). Although ALD is generally used to grow a continuous film, the SEM top views show nanoparticles uniformly spread over the samples. This is due to the high difference of surface energies between the metal and the oxidized support.[41] This has been clearly illustrated by the study of the selective Pt growth over Pd clusters that were previously deposited on Al_2O_3.[42] The authors report that the Pt nucleation occurs selectively onto the Pd clusters because the nucleation on alumina is not thermodynamically favored. In the present work, almost no Pd is detected by SEM or XRD for

$N < 200$ cycles. A nucleation delay of several hundreds of cycles has been observed for Pd deposition onto Al_2O_3 from $Pd(hfac)_2$ and formalin or H_2.[39, 42] This has been ascribed to the surface poisoning by the precursor ligands that hinders the Pd nucleation step.[40]

The particle size has been evaluated from the various SEM images and the size distributions are plotted, for each N, as insets on Figure 2. The average particle size (D_{Pd}) is then plotted in Figure 3. As expected D_{Pd} increases with N since the growth of the existing particles occurs more likely than the nucleation of additional clusters on the oxidized surface. D_{Pd} varies from 6.5 ± 1 to 25 ± 3 nm for N ranging from 400 to 900 cycles. After an incubation time of approximately 600 cycles, D_{Pd} increases linearly. The growth rate, deduced from the slope between 700 and 900 cycles, is 0.7 Å/cycle. It is notably higher than the growth rate of 0.21 Å/cycle determined in a previous work[39] by quartz crystal microbalance (QCM) for Pd deposition onto Al_2O_3. This discrepancy can be explained because, in the present work, the rate corresponds to the average particle size while the growth rate given by Elam et al.[39] corresponds to the thickness evolution calculated from the QCM data for a homogeneous film. Nevertheless, the evolutions are in agreement and both depict the same deposition process, i. e., an incubation delay due to the oxidized nature of the substrate and an island growth mechanism.

In order to demonstrate the full coverage of the TNTs by the Pd, SEM and TEM cross sections have been performed on the nanotubes after ALD of Pd. Figure 4a shows a side view of the TNTs after Pd growth. It appears distinctly on the micrograph that the external walls of the tubes are completely coated by the metallic nanoparticles. It indicates that the Pd deposition even proceeds within the narrow interstitial voids.

During the sample cutting, it is unlikely that the nanotubes are sliced along their longitudinal axis. Hence, it is almost impossible to observe, by SEM, the inner coverage of the tubes by the

Pd clusters. The TEM cross section presented in Figure 4b reveals, conversely, the presence of Pd nanoparticles within the TNTs even at the bottom part of the tubes (see the arrows on Figure 4b). This demonstrates clearly that the ALD process uniformly and fully coats the TNTs.

Figure 5 shows TEM observations of Pd clusters deposited on the TNTs after 500 ALD cycles. A general view of a tube mouth decorated by Pd clusters is shown in Figure 5a. The underlying TiO_2 is pointed out by the blue shadow. It confirms that the deposition occurs on both sides of the tube walls. The size distribution of the Pd particles is relatively homogeneous and the average size, around 7-8 nm, is in the same range as the one observed, by SEM, on Figure 2. The high-resolution view of the deposit (Figure 5b) reveals the crystal planes of the particles and confirms crystalline nature of the Pd deposit. The particles look relatively homogeneous and are mainly single-crystalline. The selected area electron diffraction (SAED) carried out on the region is presented in Figure 5c. Numerous diffraction spots and rings are visible on the pattern. The diffraction rings are attributed to the Pd while the diffraction spots are ascribed to the anatase. It indicates that the amount of underlying TiO_2 is very small. No preferential orientation is noticed in the table (shown in Supporting Information, S1) that lists the crystal planes detected by the SAED since all the main diffraction planes are visible for both materials.

Figure 6a displays the x-ray diffraction patterns of TNTs after Pd deposition for increasing number of cycles (N = 300, 400, 500 and 600 cycles). The peaks have been identified according to the reference databases (JCPDS #046-1043, JCPDS #044-1294). The diffraction peaks are mainly attributed to the Ti substrate and no TiO_2 is detected since as-grown TNTs are amorphous.[14] The diffraction peak located at 46.65° can be attributed to the Pd(200) planes while the peak positioned around 40.1° corresponds to the sum of Pd(111) and Ti(101) signals (40.12 and 40.17°, respectively). The evolution of the intensity of these peaks is presented in the insets

(Figures 6b and 6c). In both cases, the linear increase with *N* (see Supporting Information, S2) indicates that the Pd load is directly related to the number of cycles. The FWHM of the peaks decreases with the *N*. It qualitatively verifies the enlargement of particles observed previously on the SEM images. It is indeed not possible to use the Scherrer formula to evaluate the particle mean size because the main peak for Pd, the (111) plane, is located at the same diffraction angle of the Ti(101) and the intensity of the Pd(200) peak is too weak for a consistent quantitative analysis.

The surface composition of the Pd nanoparticles has been investigated by XPS. The characterizations were carried out on Pd/TNTs ($N = 500$ cycles) before and after the electrochemical measurements and the recorded peaks are shown in Figure 7. In the case of the as-prepared sample the deconvoluted Pd3d peak (Figure 7a, upper spectra) shows only one component at 335.4 eV ($Pd3d_{5/2}$) that is attributed to Pd atoms in the metallic state. [43] The analysis of the corresponding Ti2p (Figure 7b, upper spectra) shows the existence of a peak at 459.3 eV characteristic of titanium atoms in the 4+ oxidation state in TiO_2.[36] The peak measured in the O1s region (Figure 7c, upper spectra) is the result of the overlapping of the O1s peak ascribed to TiO_2 and the $Pd3p_{3/2}$. Thus, the two characteristic features of the peak at around 530.5 and 532.4 eV are due to these two contributions, respectively.[36, 44]

After the electrochemical studies a significant amount of potassium was detected on the surface as indicated by the intense K2p peak that is detected around 293.5 eV ($K2p_{3/2}$, not shown here). The deconvolution of the Pd3d peak (Figure 7a, lower spectra) reveals that beyond the component at lower BEs ($Pd3d_{5/2}$: 335.1 eV) due to metallic Pd, two additional peaks are present at higher BEs (336.1 and 337.2 eV). These two peaks are attributed to palladium in the 2+ and 4+ oxidation states due to PdO and PdO_2 and/or respective hydroxides.[45-46] It is therefore evident

that after the electrochemical measurements, oxidation of palladium has taken place and around 40% of the detected signal is due to these oxygenated species. It should be mentioned that the signal of the Pd3d peak is almost one order of magnitude lower as compared to the signal of the as-prepared sample. This decrease is due to the presence of the potassium layer over Pd/TNTs sample, which is formed from the KOH electrolyte solution used during the ethanol electrooxidation measurements. The decrease of the Pd3d signal is accompanied by a steep decrease of Ti2p signal. More specifically, after ethanol electrooxidation, the Ti2p peak becomes rather ill defined (Figure 7b, lower spectra). At the same time, the O1s component at around 530.5 eV, which is attributed to the titanium dioxide, disappears. All these observations further support the fact that potassium covers the sample diminishing the signal of both Pd and TNT support. Nevertheless, the intensity of the peak detected in the $Pd3p_{3/2}$/O1s region for the sample after the electrochemical measurements does not show a respective decrease as it would be expected due to the potassium overlayer. Based on the fact that the second component of the Pd3p doublet at around 560.2 eV ($Pd3p_{1/2}$, not shown here) is of very low intensity and because the intensity ratio of the two components should be 2, $I_{Pd3p3/2}$:$I_{Pd3p1/2}$ = 2:1,[43] we conclude that the relatively intense peak at around 532.5 eV is not due to Pd but represents surface oxygen atoms that form palladium oxides and/or hydroxides after the electrochemical measurement. At this point we cannot exclude the formation of surface complexes that contain potassium as well. The $K2p_{3/2}$ is detected around 293.4 eV. In the literature this binding energy is reported for potassium atoms in ionic compounds[43] and K/Pd. It is also well known that all alkali metals including potassium form oxopalladates (K_nPdO_m).[47] Further investigation is necessary to obtain a better insight of the K-based surface species.

As mentioned before, as-grown TNTs are mainly amorphous. A phase transformation to anatase occurs after an annealing in air at $T = 450°C$ for 2 h. The anatase exhibits the highest electron conductivity and higher O^{2-} content.[48-49] It can therefore influence strongly the electroactivity of the supported Pd catalysts. In the following, the electrochemical response of the Pd/TNTs systems has thus been investigated using either as-anodized or annealed nanotubes. Figure 8 presents the comparison of two Pd deposits carried out under the same ALD conditions ($N = 500$ cycles) on as-grown and annealed nanotubes, respectively. The comparison of the SEM micrographs attests that there is no morphological difference between the two Pd films. Similarly, XPS and XRD investigations also confirm that neither chemical nor the crystalline variations are observed for the Pd deposit depending on the thermal treatment of the substrates. This allows a direct comparison of the electrocatalytic activity of Pd deposited on amorphous and on crystalline TNTs, as shown in the following section.

Ethanol Electrooxidation

Figure 9 shows cyclic voltammograms of Pd/TNTs samples containing 400, 500, 700 and 900 ALD cycles of Pd deposited on both as grown (solid line) and annealed (dashed line) TNTs in 1 M KOH (the reference CVs for bare TNTs are shown in Figure S3 in supporting information). For 400 ALD Pd/TNTs and samples with lower ALD cycles, the response of Pd is absent from the CVs. For samples of 500, 700 and 900 ALD cycles, the characteristic peaks of Pd oxidation and reduction as well as hydrogen evolution region are present on CVs. The absence of the Pd response for samples with low Pd loading, i. e., small clusters, could be a result of the SMSI effect in Pd/TNTs. SMSI is of either electronic or geometric type, latter also called decoration model.[9, 50] In the decoration model, the SMSI is a result of the back spillover of the partially reduced TiO_x species onto the surface of metal catalysts, which takes place when the catalyst is

reduced in hydrogen at high temperature. As defined in the metal-semiconductor boundary layer theory, at thermodynamic equilibrium the Fermi energy level of electrons of the two materials in contact is equal. When two materials with different Fermi level (work function) put in contact, charge is transported from the material with the lower work function to the material with the higher work function. The work function of anatase TiO_2 is 5.1 eV[51] and Pd 5.2-5.4 eV for bulk Pd and even higher for nanoparticles.[52-53] Upon contact the negative charge is transported from TiO_2 to Pd. Therefore, O^{2-} and/or OH^- migration from TiO_2 onto Pd surface is expected. In the "oxygen vacancy model" developed by Sanchez and Gasquez,[54] the metal diffusion into support bulk vacancies and complete or partial burial of small metal crystallites were proposed. In addition, surface migration of O^{2-} and/or OH^- can cover the metal clusters or strands bringing about complete elimination of sorptive and catalytic properties.[54] It is suggested that in the case of small Pd clusters, Pd atoms become buried into TiO_2 support and covered by O^{2-}/OH^-, therefore fraction of accessible atoms is small and their sorptive and catalytic properties are affected negatively. As the particle size increases, the Pd-TiO_2 interaction diminishes and Pd atoms situated further from the support remain accessible to surrounding electrolyte and show similar CV profile as for bulk Pd electrode (Figure 9b-d).[55] The anodic current growth at potentials more positive than – 0.2 V (Figure 9b, 9c, 9d) is due to the formation of Pd-OH, PdO and PdO_x that are developed successively as the potential becomes more positive. The cathodic peak centered at around – 0.2 V is due to the reduction of the Pd oxides formed on the anodic scan. The intensity of this peak depends on the maximum anodic potential, because a more complete oxide layer and higher valence oxides are formed at higher potentials. At potentials more negative than – 0.4 V the region of hydrogen adsorption/absorption and desorption is situated.[56]

For Pd/TNTs with 500 ALD cycles, the current density is significantly higher for the annealed support confirming that the changes in TiO_2 properties have a greater effect on smaller Pd clusters of lower loading (shown in Figure 2) than larger Pd deposits obtained at 700 and 900 ALD cycles. The annealing of TiO_2 nanotubes in air at 450°C results in anatase structure with high conductivity.[57] For samples containing 700 and 900 ALD cycles, the current densities are comparable for as-grown and annealed samples (Figure 9 c,d), but much lower than for 500 ALD. As was shown previously for Pt deposited on TiO_2 nanotubes,[58-59] the increase of the Pt amount led to the decrease of MSI effect, therefore affecting the catalytic properties of Pt to a lesser degree. The similar effect could be in play for Pd/TNTs of 700 and 900 ALD cycles. Furthermore, as the cluster size increases to 900 ALD cycles the current density decreases significantly if compared to Pd/TNTs of 700 and 500 ALD cycles. It can be also seen (Figure 9c) that annealing of the support not only affects the current values but also the ease of PdO_x formation and reduction. For instance, after annealing the peak of Pd oxidation decreases and shifts to higher anodic potentials, indicating that annealed-TNTs stabilize Pd in the metallic state, as also seen in the positive shift of PdO_x reduction peak confirming that this process is more thermodynamically favorable on the annealed Pd/TNTs with 700 ALD cycles. In an earlier work,[15] Pd reduction peak was observed between 0.6 and 0.7 V vs RHE (– 0.341 and – 0.241 V vs Hg/HgO) on Pd nanoparticles prepared by electrochemical milling of the larger Pd clusters. In another report,[17] the reduction peak maximum was situated at – 0.45 V vs SCE (– 0.307 V vs. Hg/HgO). The reported potentials are more negative that ones observed in the present work indicating that charge transfer between Pd and TNTs and/or Pd interaction with O^{2-} bulk vacancies make the reduction of Pd oxides easier.

Figure 10 compares electrocatalytic activity of the two catalysts with the same Pd loading (i. e., $N = 500$ cycles) but deposited on as-grown and annealed TNTs for ethanol electrooxidation. The current density is much higher for Pd catalysts deposited on the annealed support and increases in the whole range of the anodic potentials, whereas for as-grown Pd/TNTs system, the maximum current density is reached at 0.15 V following by the catalyst deactivation due to oxide formation. The increase in the current density for annealed TNTs is due to the increased conductivity of the anatase structured TiO_2 nanotubes over the amorphous TiO_2 nanotubes.[60] Therefore, the further studies of the effect of Pd loading were carried out on annealed TNTs.

The three Pd/TNTs catalysts with 500, 700 and 900 ALD cycles were tested for ethanol electrooxidation and the resulting cyclic voltammograms are shown in Figure 11. The current densities are given per geometric area and ECSA on Figure 11a and 11b, respectively. As the number of ALD cycles increases the particle size increases as shown in Figure 2 and confirmed by XRD measurements, which in turn will influence the available active surface area. Therefore, in order to compare the intrinsic activity of Pd/TNTs prepared with different number of ALD cycles, the ECSA of Pd/TNTs catalysts was estimated using PdO reduction peak in H_2SO_4[61] (Figure S4 in supporting information). The distinct PdO reduction peak in acid media makes the calculation of the charge required to oxidize the monolayer of PdO more straightforward and accurate than in alkaline media.[61] It is accepted that the reduction charge of a full monolayer of Pd monoxide is 420 $\mu C\ cm^{-2}$.[62-65] The formation of Pd oxide at a fixed cathodic potential is a function of time and the PdO reduction charge reaches the plateau in the region where a complete PdO monolayer is formed.[65] The estimated ECSA, for Pd deposited on annealed TiO_2 nanotubes with 500, 700 and 900 ALD cycles is 22.3, 29.6 and 7.1 cm^2, respectively. The ECSA

increases as number of cycle increases from 500 to 700. At the same time, the average nanoparticle size increases as well from 7 till 11 nm indicating that ECSA increase is not purely geometric but an interaction with TiO_2 support and formation of new active sites probably occur. Furthermore, the particle distribution and interparticle distance have larger contribution towards ECSA than Pd particle size on its own. The significant decrease of ECSA for 900 ALD cycles is due to the formation of the larger coalesced Pd clusters with lower surface area (average size of 25 nm, Figure 2) and/or partial obstruction of the 3D nanostructure of TNTs by large Pd clusters.

Figure 11 shows that when current density is normalized by geometric area, its amplitude for 500 and 700 ALD cycles is the same up to 0.3 V, where the sample covered by 700 cycles deactivates rapidly due to Pd oxidation, while the current density continues to increase up to 0.36 V for $N = 500$ cycles On the reverse scan all three catalyst remain inactive till – 0.15 V, because more negative potentials are required to reduce PdO_x, which is not a catalyst for ethanol electrooxidation.

The comparison of the intrinsic activity of the three Pd/TNTs catalysts (Figure 11b) shows that the sample covered by 500 cycles Pd exhibits the highest current density in the entire potential region in both forward and backward scans, also it remains active till higher potentials if compare to two other catalysts. The catalyst with 900 ALD cycles has a much lower activity due to the larger particle size and partial closing of the TNTs. In order to compare the present results with literature, the Pd load (i. e. the mass of Pd, m_{Pd}, per area unit) has been estimated from the ECSA and the D_{Pd}. Using these two experimental measurements, it has been possible to estimate the particle density (N_{Pd}) and m_{Pd}. The m_{Pd} is 31, 76 and 35 $\mu g \cdot cm^{-2}$, for a number of 500, 700 and 900 ALD cycles, respectively. The m_{Pd} for 500 and 700 ALD cycles appear realistic. However, the low value for 900 ALD cycles shows, of course, the limitation of the calculation when the

particles merge (since the ECSA is a superficial measurement it cannot be used to calculate accurately the mass of a continuous Pd film). Nevertheless, the m_{Pd} for 500 ALD is the most interesting for comparisons since it exhibits the highest activity. The peak current for ethanol oxidation is approximately 2.25 A mg^{-1} for 500 ALD cycles. The comparison of this electroactivity with literature is thus promising. Qin et al.[17] reported for Pd deposited into TNTs an oxidation current of ca. 6 A mg^{-1} with CVs performed at a higher scan rate (50 mV s^{-1}). Similarly, Chen et al.[15] have measured an oxidation current of ca. 9 A mg^{-1} but the experiments were carried out in a more concentrated solution ($c_{ethanol}$ = 2.2 mol L^{-1}) and the scan rate was also two times higher (50 mV s^{-1}). The comparison with Pd catalysts deposited by ALD on porous carbon is even more promising. Rikkinen et al.[32] have indeed reported an electroactivity 4.5 times higher than commercial materials, but the oxidation current remains four times lower than the present study with a current of 0.5 A mg^{-1} at 0.75 V vs. RHE.[32]

Figure 12 shows chronoamperograms of Pd catalysts with various loading deposited on annealed TNTs at – 0.2 V. For the sample with 900 ALD cycles, the current density starts at 0.13 mA cm^{-2} and diminishes very fast until it reaches a steady-state at about 0.03 mA cm^{-2}. The samples with 500 and 700 cycles show higher initial current density values of 0.25 and 0.20 mA cm^{-2}, respectively, however the current density continues to decrease without reaching a steady-state even after 1 h. The current decrease is due to poisoning of the Pd surface active sites by adsorbed ethoxy (CH_3CH_2O) or other poisonous (C2) intermediates.[8, 66] The decay could be also associated with PdO_x formation, confirmed by the XPS measurements of the Pd/TNTs after ethanol electrooxidation (Figure 7). XPS showed that palladium in the 2+ and 4+ oxidation states was formed. In addition, as shown by XPS, the formation of oxopalladate (K_nPdO_m) complexes cannot be ruled out. Therefore, the above effects would gradually decrease the

number of active sites and lead to the continuous current decay. The current percentage loss, after double layer correction, is 71.6, 57.3 and 40.1% for 500, 700 and 900 ALD of Pd, respectively.

CA measurements showed that the samples with 500 and 700 cycles are more active, at least during the first hours of operation, while the sample with 900 cycles shows a much lower catalytic activity under the same operating conditions but it reaches quickly (after 1500 s) a steady-state around 0.03 mA cm^{-2}. The levels of the current densities are in agreement with CVs experiments shown in Figure 11b (where a vertical dashed line indicate the potential corresponding to the CA experiments).

The electrochemical measurements showed that Pd deposited using 500 ALD cycles (average particle size of 6.5 nm) on annealed TNTs has the optimum electrocatalytic performance. For samples with lower ALD cycles, no electrochemical response was detected for both annealed and as-grown samples. It is proposed that SMSI results in the coverage and/or burial of small Pd clusters into TiO_2 nanotubes. This effectively negated sorptive and catalytic properties of Pd deposited using 400 and fewer ALD cycles. For Pd/TNTs electrocatalysts of 700 and 900 ALD cycles, it is suggested that both larger particle size, implying the lower active surface area, as well as weaker electronic interaction between Pd clusters and TiO_2 nanotubes was responsible for lower catalytic activity.

Conclusion

In the present work we show that ALD can be successfully used to functionalize TNTs with Pd nanoparticles for ethanol electrooxidation. The particle size is precisely controlled by the number of ALD cycles and the catalysts fully cover the inner and outer walls of the nanotubes. ALD allows the use of a controlled amount of Pd and can thus decrease the costs. The influence of the

substrate on the catalyst activity has been demonstrated trough the modification of the crystalline structure of the TNTs. The electrooxidation of ethanol is indeed strongly enhanced when the TiO_2 is annealed since anatase is more conductive than the amorphous TiO_2. Catalysts with the different number of ALD cycles were prepared. It was found by SEM and XRD that Pd forms well-defined and crystalline nanoparticles with face-centred cubic (fcc) structure on entire surface of TNTs. The particle and crystallite size increases with the number of ALD cycles. XPS analysis showed that as prepared Pd nanoparticles are present in metallic state, whereas after ethanol electrooxidation 40% of surface Pd is transformed to PdO_x. Among the prepared electrocatalysts (N = 400 – 900 ALD cycles), the 500 ALD Pd/TNTs system showed the best catalytic activity and satisfactory stability in alkaline media. The electrochemical characterizations have demonstrated that these Pd/TNTs systems exhibit high current densities and low onset potential if compared to the literature and commercial catalysts. The use of ALD to grow metallic nanoparticles onto three-dimensional nanostructured substrates appears to be a very promising approach for preparation of well-defined catalysts for ethanol and other alcohol electrooxidation.

ASSOCIATED CONTENT

Supporting Information. Indexing of the selected area electron diffraction for Pd nanoparticles deposited on TNTs. Evolution of the diffraction peaks (2θ = 40.1° and 46.5°) with N. Electrochemical behavior of the bare TNTs. Cyclic voltammetry of Pd/TNTs in 0.5 M H_2SO_4 used for ECSA estimation. This material is available free of charge via the Internet at http://pubs.acs.org.

AUTHOR INFORMATION

Corresponding Author

*To whom correspondence should be addressed: elena.baranova@uottawa.ca; lionel.santinacci@univ-amu.fr

Present Addresses

§ Université Paris Sud - CNRS, Institut de Chimie Moléculaire et des Matériaux d'Orsay, Rue du Doyen Georges Poitou, F-91405 Orsay, France.

Author Contributions

The manuscript was written through contributions of all authors.

$^{\perp}$ These authors contributed equally.

ACKNOWLEDGMENT

The authors acknowledge D. Chaudanson, S. Nitsche (CINaM) and Y. Yamamoto (JEOL France for the SEM pictures obtained with the JEOL 7800F) for their precious help with the electron microscopy and V. Heresanu (CINaM) for XRD measurements and interpretation. A. Baronnet (CINaM) is also acknowledged for fruitful discussions. This collaborative work was supported by the France-Canada Research Fund. M. K. S. Barr and L. Assaud are indebted to the Conseil Régional Provence-Alpes-Côte d'Azur and the CNRS for the PhD grants.

REFERENCES

(1) Bianchini, C.; Shen, P. K., Palladium-Based Electrocatalysts for Alcohol Oxidation in Half Cells and in Direct Alcohol Fuel Cells. *Chem. Rev.* **2009,** *109*, 4183-4206.

(2) Antolini, E., Catalysts for Direct Ethanol Fuel Cells. *J. Power Sources* **2007,** *170*, 1-12.

(3) Dillon, R.; Srinivasan, S.; Arico, A.; Antonucci, V., International Activities in Dmfc R&D: Status of Technologies and Potential Applications. *J. Power Sources* **2004,** *127*, 112-126.

(4) Antolini, E., Palladium in Fuel Cell Catalysis. *Energy Environ. Sci.* **2009,** *2*, 915-931.

(5) Bambagioni, V.; Bianchini, C.; Marchionni, A.; Filippi, J.; Vizza, F.; Teddy, J.; Serp, P.; Zhiani, M., Pd and Pt–Ru Anode Electrocatalysts Supported on Multi-Walled Carbon Nanotubes and Their Use in Passive and Active Direct Alcohol Fuel Cells with an Anion-Exchange Membrane (Alcohol = Methanol, Ethanol, Glycerol). *J. Power Sources* **2009,** *190*, 241-251.

(6) Feng, Y.-Y.; Liu, Z.-H.; Xu, Y.; Wang, P.; Wang, W.-H.; Kong, D.-S., Highly Active Pdau Alloy Catalysts for Ethanol Electro-Oxidation. *J. Power Sources* **2013,** *232*, 99-105.

(7) Monyoncho, E. A.; Ntais, S.; Soares, F.; Woo, T. K.; Baranova, E. A., Synergetic Effect of Palladium–Ruthenium Nanostructures for Ethanol Electrooxidation in Alkaline Media. *J. Power Sources* **2015,** *287*, 139-149.

(8) Neto, A. O.; da Silva, S. G.; Buzzo, G. S.; de Souza, R. F. B.; Assumpção, M. H. M. T.; Spinacé, E. V.; Silva, J. C. M., Ethanol Electrooxidation on Pdir/C Electrocatalysts in Alkaline Media: Electrochemical and Fuel Cell Studies. *Ionics* **2015,** *21*, 487-495.

(9) Tauster, S. J.; Fung, S. C.; Garten, R. L., Strong Metal-Support Interactions - Group-8 Noble-Metals Supported on Tio_2. *J. Am. Chem. Soc.* **1978,** *100*, 170-175.

(10) Hepel, M.; Kumarihamy, I.; Zhong, C. J., Nanoporous Tio2-Supported Bimetallic Catalysts for Methanol Oxidation in Acidic Media. *Electrochem. Commun.* **2006,** *8*, 1439-1444.

(11) Ntais, S.; Isaifan, R. J.; Baranova, E. A., An X-Ray Photoelectron Spectroscopy Study of Platinum Nanoparticles on Yttria-Stabilized Zirconia Ionic Support: Insight into Metal Support Interaction. *Mater. Chem. Phys.* **2014,** *148*, 673-679.

(12) Zhang, J.; Cheng, Y.; Lu, S.; Jia, L.; Shen, P. K.; Jiang, S. P., Significant Promotion Effect of Carbon Nanotubes on the Electrocatalytic Activity of Supported Pd Nps for Ethanol Oxidation Reaction of Fuel Cells: The Role of Inner Tubes. *Chem. Commun.* **2014,** *50*, 13732-13734.

(13) Huang, S.-Y.; Ganesan, P.; Park, S.; Popov, B. N., Development of a Titanium Dioxide-Supported Platinum Catalyst with Ultrahigh Stability for Polymer Electrolyte Membrane Fuel Cell Applications. *J. Am. Chem. Soc.* **2009,** *131*, 13898-13899.

(14) Lee, K.; Mazare, A.; Schmuki, P., One-Dimensional Titanium Dioxide Nanomaterials: Nanotubes. *Chem. Rev.* **2014,** *114*, 9385-9454.

(15) Chen, Y.-X.; Lavacchi, A.; Chen, S.-P.; di Benedetto, F.; Bevilacqua, M.; Bianchini, C.; Fornasiero, P.; Innocenti, M.; Marelli, M.; Oberhauser, W.; Sun, S.-G.; Vizza, F., Electrochemical Milling and Faceting: Size Reduction and Catalytic Activation of Palladium Nanoparticles. *Angew. Chem. Int. Ed.* **2012,** *51*, 8500-8504.

(16) Xu, W.; Zhu, S.; Li, Z.; Cui, Z.; Yang, X., Synthesis and Catalytic Properties of Pd Nanoparticles Loaded Nanoporous Tio2 Material. *Electrochim. Acta* **2013,** *114*, 35-41.

(17) Qin, Y.-H.; Yang, H.-H.; Lv, R.-L.; Wang, W.-G.; Wang, C.-W., Tio2 Nanotube Arrays Supported Pd Nanoparticles for Ethanol Electrooxidation in Alkaline Media. *Electrochim. Acta* **2013,** *106*, 372-377.

(18) Elam, J. W.; Routkevitch, D.; Mardilovich, P. P.; George, S. M., Conformal Coating on Ultrahigh-Aspect-Ratio Nanopores of Anodic Alumina by Atomic Layer Deposition. *Chem. Mater.* **2003,** *15*, 3507-3517.

(19) Hausmann, D.; Becker, J.; Wang, S.; Gordon, R. G., Rapid Vapor Deposition of Highly Conformal Silica Nanolaminates. *Science* **2002,** *298*, 402-406.

(20) Moyen, E.; Santinacci, L.; Masson, L.; Wulfhekel, W.; Hanbücken, M., A Novel Self-Ordered Sub-10 Nm Nanopore Template for Nanotechnology. *Adv. Mater.* **2012,** *24*, 5094–5098.

(21) Detavernier, C.; Dendooven, J.; Sree, S. P.; Ludwig, K. F.; Martens, J. A., Tailoring Nanoporous Materials by Atomic Layer Deposition. *Chem. Soc. Rev.* **2011,** *40*, 5242-5253.

(22) Elam, J. W.; Dasgupta, N. P.; Prinz, F. B., Ald for Clean Energy Conversion, Utilization, and Storage. *MRS Bull.* **2011,** *36*, 899-906.

(23) Lu, J.; Elam, J. W.; Stair, P. C., Synthesis and Stabilization of Supported Metal Catalysts by Atomic Layer Deposition. *Acc. Chem. Res.* **2013,** *46*, 1806-1815.

(24) Goldstein, D. N.; George, S. M., Enhancing the Nucleation of Palladium Atomic Layer Deposition on Al2o3 Using Trimethylaluminum to Prevent Surface Poisoning by Reaction Products. *Appl. Phys. Lett.* **2009,** *95*, 143106.

(25) Assaud, L.; Schumacher, J.; Tafel, A.; Bochmann, S.; Christiansen, S.; Bachmann, J., Systematic Increase of Electrocatalytic Turnover at Nanoporous Platinum Surfaces Prepared by Atomic Layer Deposition. *J. Mater. Chem. A* **2015,** *3*, 8450-8458.

(26) Feng, H.; Libera, J. A.; Stair, P. C.; Miller, J. T.; Elam, J. W., Subnanometer Palladium Particles Synthesized by Atomic Layer Deposition. *ACS Catal*. **2011,** *1*, 665-673.

(27) Lu, J.; Liu, B.; Greeley, J. P.; Feng, Z.; Libera, J. A.; Lei, Y.; Bedzyk, M. J.; Stair, P. C.; Elam, J. W., Porous Alumina Protective Coatings on Palladium Nanoparticles by Self-Poisoned Atomic Layer Deposition. *Chem*. *Mater*. **2012,** *24*, 2047-2055.

(28) Su, C.-Y.; Hsueh, Y.-C.; Kei, C.-C.; Lin, C.-T.; Perng, T.-P., Fabrication of High-Activity Hybrid Pt@Zno Catalyst on Carbon Cloth by Atomic Layer Deposition for Photoassisted Electro-Oxidation of Methanol. *J*. *Phys*. *Chem*. *C* **2013,** *117*, 11610-11618.

(29) Jukk, K.; Kongi, N.; Tarre, A.; Rosental, A.; Treshchalov, A. B.; Kozlova, J.; Ritslaid, P.; Matisen, L.; Sammelselg, V.; Tammeveski, K., Electrochemical Oxygen Reduction Behaviour of Platinum Nanoparticles Supported on Multi-Walled Carbon Nanotube/Titanium Dioxide Composites. *J*. *Electroanal*. *Chem*. **2014,** *735*, 68-76.

(30) Chih-Chieh, W.; Yang-Chih, H.; Chung-Yi, S.; Chi-Chung, K.; Tsong-Pyng, P., Deposition of Uniform Pt Nanoparticles with Controllable Size on Tio 2 -Based Nanowires by Atomic Layer Deposition and Their Photocatalytic Properties. *Nanotechnology* **2015,** *26*, 254002.

(31) Feng, H.; Elam, J. W.; Libera, J. A.; Setthapun, W.; Stair, P. C., Palladium Catalysts Synthesized by Atomic Layer Deposition for Methanol Decomposition. *Chem*. *Mater*. **2010,** *22*, 3133-3142.

(32) Rikkinen, E.; Santasalo-Aarnio, A.; Airaksinen, S.; Borghei, M.; Viitanen, V.; Sainio, J.; Kauppinen, E. I.; Kallio, T.; Krause, A. O. I., Atomic Layer Deposition Preparation of Pd

Nanoparticles on a Porous Carbon Support for Alcohol Oxidation. *J. Phys. Chem. C* **2011,** *115*, 23067-23073.

(33) Assaud, L.; Monyoncho, E.; Pitzschel, K.; Allagui, A.; Petit, M.; Hanbuecken, M.; Baranova, E. A.; Santinacci, L., 3d-Nanoarchitectured Pd/Ni Catalysts Prepared by Atomic Layer Deposition for the Electrooxidation of Formic Acid. *Beilstein J. Nanotechnol.* **2014,** *5*, 162-172.

(34) Richter, K.; Peplinski, B., Energy Calibration of Electron Spectrometers. *J. Electron. Spectrosc. Relat. Phenom.* **1978,** *13*, 69-71.

(35) Hüfner, S.; Wertheim, G. K., Core-Line Asymmetries in the X-Ray-Photoemission Spectra of Metals. *Phys. Rev. B* **1975,** *11*, 678-683.

(36) Ntais, S.; Dracopoulos, V.; Siokou, A., $Ticl_4(Thf)_2$ Impregnation on a Flat Sio_x/Si(100) and on Polycrystalline Au Foil: Determination of Surface Species Using Xps. *J. Mol. Catal. A: Chem.* **2004,** *220*, 199-205.

(37) Czerwinski, A., The Adsorption of Carbon Oxideson a Palladium Electrode from Acidic Solution *J. Electroanal. Chem.* **1994,** *379*, 487-493.

(38) Assaud, L.; Heresanu, V.; Hanbuecken, M.; Santinacci, L., Fabrication of P/N Heterojunctions by Electrochemical Deposition of Cu_2o onto Tio2 Nanotubes. *C. R. Chim.* **2013,** *16*, 89-95.

(39) Elam, J. W.; Zinovev, A.; Han, C. Y.; Wang, H. H.; Welp, U.; Hryn, J. N.; Pellin, M. J., Atomic Layer Deposition of Palladium Films on Al2o3 Surfaces. *Thin Solid Films* **2006,** *515*, 1664-1673.

(40) Goldstein, D. N.; George, S. M., Surface Poisoning in the Nucleation and Growth of Palladium Atomic Layer Deposition with Pd(Hfac)2 and Formalin. *Thin Solid Films* **2011,** *519*, 5339-5347.

(41) Campbell, C. T., Ultrathin Metal Films and Particles on Oxide Surfaces: Structural, Electronic and Chemisorptive Properties. *Surf. Sci. Rep.* **1997,** *27*, 1-111.

(42) Weber, M. J.; Mackus, A. J. M.; Verheijen, M. A.; van der Marel, C.; Kessels, W. M. M., Supported Core/Shell Bimetallic Nanoparticles Synthesis by Atomic Layer Deposition. *Chem. Mater.* **2012,** *24*, 2973-2977.

(43) Briggs, D.; Seah, M. P., Auger and X-Ray Photoelectron Spectroscopy. In *Practical Surface Analysis* 2nd ed.; Briggs, D.; Seah, M. P., Eds. John Wiley & Sons: New York, **1996**.

(44) Militello, M. C.; Simko, S. J., Elemental Palladium by Xps. *Surf. Sci. Spectra* **1994,** *3*, 387-394.

(45) Shafeev, G. A.; Themlin, J. M.; Bellard, L.; Marine, W.; Cros, A., Enhanced Adherence of Area-Selective Electroless Metal Plating on Insulators. *J. Vac. Sci. Technol. A* **1996,** *14*, 319-326.

(46) Gao, W.; Jin, R.; Chen, J.; Guan, X.; Zeng, H.; Zhang, F.; Liu, Z.; Guan, N., Titania-Supported Pd–Cu Bimetallic Catalyst for the Reduction of Nitrite Ions in Drinking Water. *Catal. Lett.* **2003,** *91*, 25-30.

(47) Griffith, W. P.; Robinson, S. D.; Swars, K., Palladium. In *Gmelin Handbook of Inorganic Chemistry*, 8th ed.; Griffith, W. P.; Swars, K., Eds. Springer-Verlag GmbH: Berlin Heidelberg **1989**.

(48) Tang, H.; Prasad, K.; Sanjinès, R.; Schmid, P. E.; Lévy, F., Electrical and Optical Properties of Tio2 Anatase Thin Films. *J. App. Phys.* **1994,** *75*, 2042.

(49) Tighineanu, A.; Albu, S. P., Conductivity of Anodic Tio_2 Nanotubes: Influence of Annealing Conditions. *Phys. Status Solidi RRL* **2014,** *8*, 158-162.

(50) Haller, G. L.; Resasco, D. E., Metal–Support Interaction: Group Viii Metals and Reducible Oxides. *Adv. Catal.* **1989,** *36*, 173-235.

(51) Xiong, G.; Shao, R.; Droubay, T. C.; Joly, A. G.; Beck, K. M.; Chambers, S. A.; Hess, W. P., Photoemission Electron Microscopy of Tio_2 Anatase Films Embedded with Rutile Nanocrystals. *Adv. Funct. Mater.* **2007,** *17*, 2133-2138.

(52) Singh-Miller, N. E.; Marzari, N., Surface Energies, Work Functions, and Surface Relaxations of Low-Index Metallic Surfaces from First Principles. *Phys. Rev. B* **2009,** *80*, 235407.

(53) Harinipriya, S.; Sangaranarayanan, M. V., Influence of the Work Function on Electron Transfer Processes at Metals: Application to the Hydrogen Evolution Reaction. *Langmuir* **2002,** *18*, 5572-5578.

(54) Sanchez, M. G.; Gazquez, J. L., Oxygen Vacancy Model in Strong Metal-Support Interaction. *J. Catal.* **1987,** *104*, 120-135.

(55) Burke, L. D.; Casey, J. K., The Electrocatalytic Behaviour of Palladium in Acid and Base. *J. Appl. Electrochem.* **1993,** *23*, 573-582.

(56) Ruvinsky, P. S.; Pronkin, S. N.; Zaikovskii, V. I.; Bernhardt, P.; Savinova, E. R., On the Enhanced Electrocatalytic Activity of Pd Overlayers on Carbon-Supported Gold Particles in Hydrogen Electrooxidation. *Phys. Chem. Chem. Phys.* **2008,** *10*, 6665–6676.

(57) Stiller, M.; Barzola-Quiquia, J.; Lorite, I.; Esquinazi, P.; Kirchgeorg, R.; Albu, S. P.; Schmuki, P., Transport Properties of Single Tio_2 Nanotubes. *Appl. Phys. Lett.* **2013,** *103*, 173108.

(58) Rettew, R. E.; Allam, N. K.; Alamgir, F. M., Interface Architecture Determined Electrocatalytic Activity of Pt on Vertically Oriented Tio2 Nanotubes. *ACS Appl. Mater. Interfaces* **2011,** *3*, 147-151.

(59) Cheng, S.; Rettew, R. E.; Sauerbrey, M.; Alamgir, F. M., Architecture-Dependent Surface Chemistry for Pt Monolayers on Carbon-Supported Au. *ACS Appl. Mater. Interfaces* **2011,** *3*, 3948-3956.

(60) Tighineanu, A.; Ruff, T.; Albu, S.; Hahn, R.; Schmuki, P., Conductivity of Tio2 Nanotubes: Influence of Annealing Time and Temperature. *Chem. Phys. Lett.* **2010,** *494*, 260-263.

(61) Horkans, J., The Hydrogen Region of the Cyclic Voltammetry of Pd: The Effect of the Ph and Anion. *J. Electroanal. Chem.* **1986,** *209*, 371-376.

(62) Chierchie, T.; Mayer, C.; Lorenz, W. J., Structural Changes of Surface Oxide Layers on Palladium *J. Electroanal. Chem.* **1982,** *135*, 211-220.

(63) Correia, A. N.; Mascaro, L. H.; Machado, S. A. S.; Avaca, L. A., Active Surface Area Determination of Pd-Si Alloys by H-Adsorption. *Electrochim. Acta* **1997,** *42*, 493-495.

(64) Juodkazis, K.; Juodkazyte, J.; Sebeka, B.; Sukienë, V., Kinetic Regularities of Cathodic Reduction of Palladium (Ii) Oxide Surface Layer. *Chemija* **2003,** *14*, 78.

(65) Rand, D. A. J.; Woods, R., The Nature of Adsorbed Oxygen on Rhodium, Palladium and Gold Electrodes. *J. Electroanal. Chem.* **1971,** *31*, 29-38.

(66) Yang, Y.-Y.; Ren, J.; Li, Q.-X.; Zhou, Z.-Y.; Sun, S.-G.; Cai, W.-B., Electrocatalysis of Ethanol on a Pd Electrode in Alkaline Media: An in Situ Attenuated Total Reflection Surface-Enhanced Infrared Absorption Spectroscopy Study. *ACS Catal.* **2014,** *4*, 798-803.

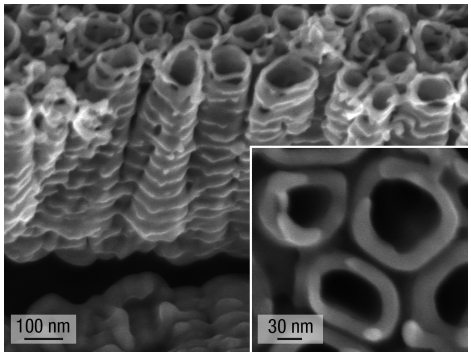

Figure 1. SEM image of TNTs grown at $U = 20$ V for 1 h in 1 M H_3PO_4 + 1 M NaOH + 0.5% HF. The inset shows a high-magnification top view of the tubes mouth.

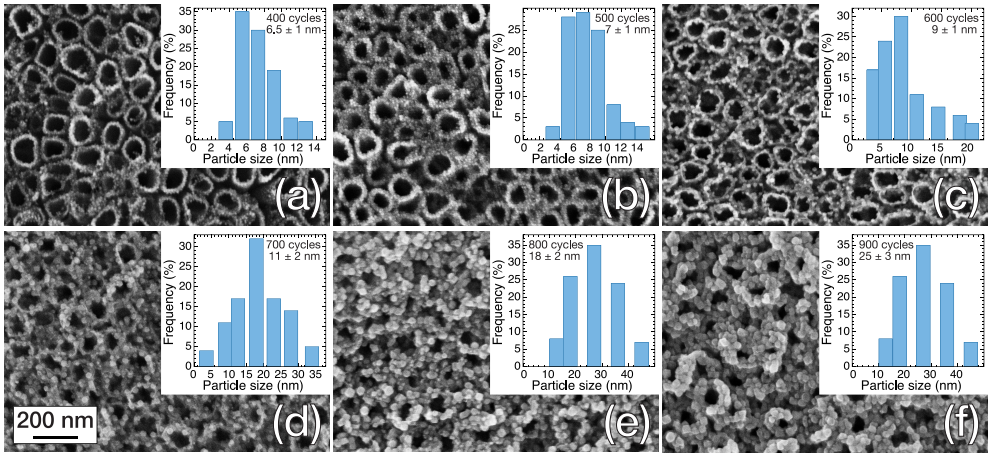

Figure 2. SEM micrographs of TNTs coated by Pd nanoparticles with increasing number of ALD cycles: (a) 400, (b) 500, (c) 600, (d) 700, (e) 800, and (f) 900 cycles. Insets show the size distribution estimated, for each *N*, from the SEM pictures.

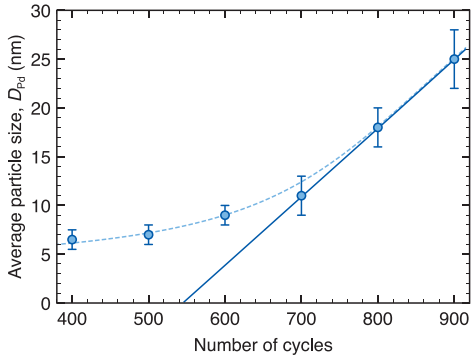

Figure 3. Evolution of the average size of Pd particles with the number of ALD cycles.

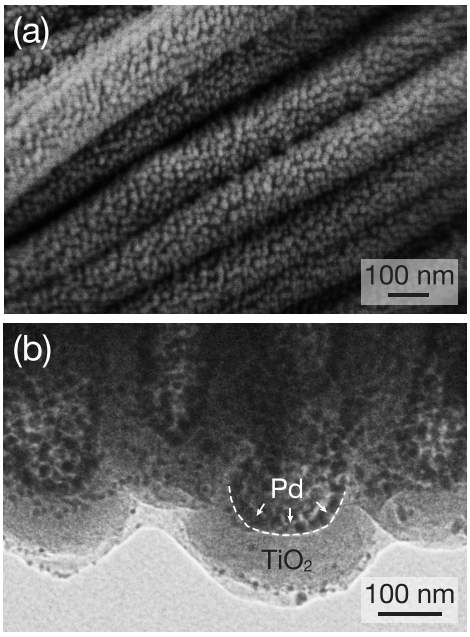

Figure 4. (a) SEM side view showing the external wall of TNTs covered by Pd nanoparticles. (b) TEM cross section of the bottom part of the TNTs after Pd deposition. The dashed line highlights the bottom part of one nanotube covered by Pd nanoparticles. $N = 700$ cycles in both cases.

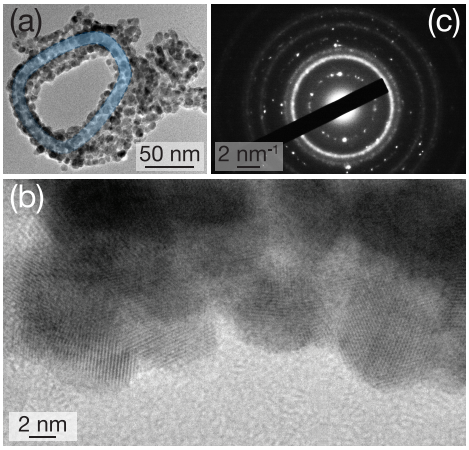

Figure 5. TEM images of Pd nanoparticles deposited (N = 500 cycles) onto TNTs after annealing at 450°C for 2 h. (a) Top view of a TNT mouth covered by Pd nanoparticles. The blue shadow highlights the position of the TNT. (b) High-resolution image of Pd particles and (c) the corresponding selected area electron diffraction.

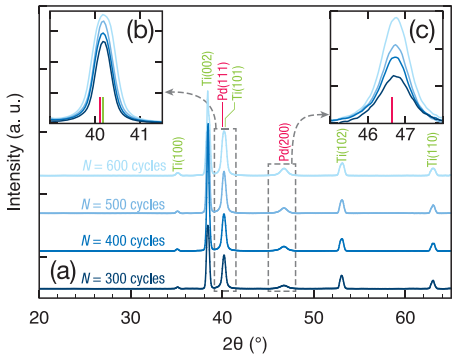

Figure 6. (a) X-ray diffractograms of TNTs after depositions of Pd nanoparticles for various number of cycles (*N* is indicated on the plot). The Pd and Ti diffraction planes are indicated on the corresponding peaks. (b) and (c) show an enlarged view of the Pd(111)/Ti(101) and Pd(200) peaks regions, respectively. The colored bars correspond to the position of the reference peaks of Pd and Ti.

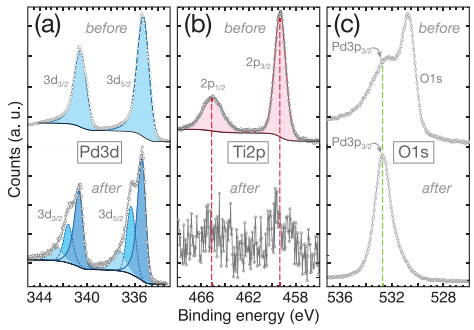

Figure 7. Pd3d (a), Ti2p (b) and O1s (c) XPS peaks before (upper spectra) and after (lower spectra) electrochemical measurements of Pd-covered TNTs (N = 500 cycles).

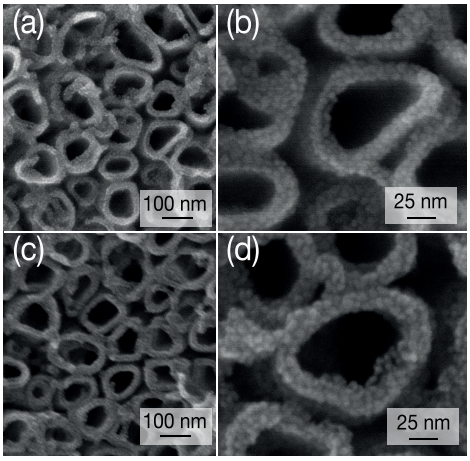

Figure 8. SEM top views of TNTs after ALD of Pd (N = 500 cycles). The Pd was deposited onto as-grown (a,b) and annealed (c,d) TNTs.

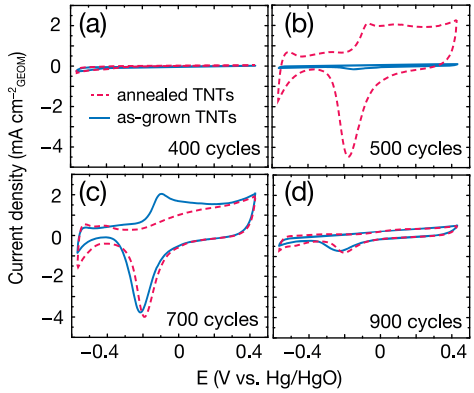

Figure 9. Cyclic voltammograms of as-grown (full line) and annealed (dashed line) TNTs after ALD of Pd for N = 400 (a), 500 (b), 700 (c) and 900 (d) cycles. The electrolyte is 1 M KOH, scan rate is 25 mV s^{-1}.

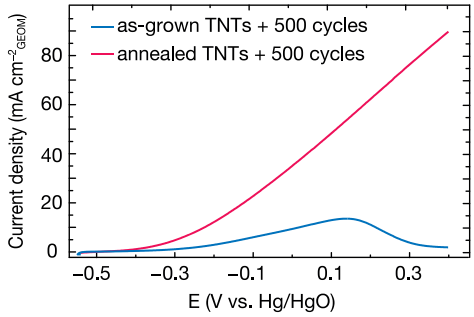

Figure 10. Cyclic voltammograms of 500 Pd ALD cycles on as-grown and annealed TNTs in 1 M KOH + 1 M C_2H_5OH. The scan rate is 25 mV s^{-1} and the current density is normalized by geometric surface area.

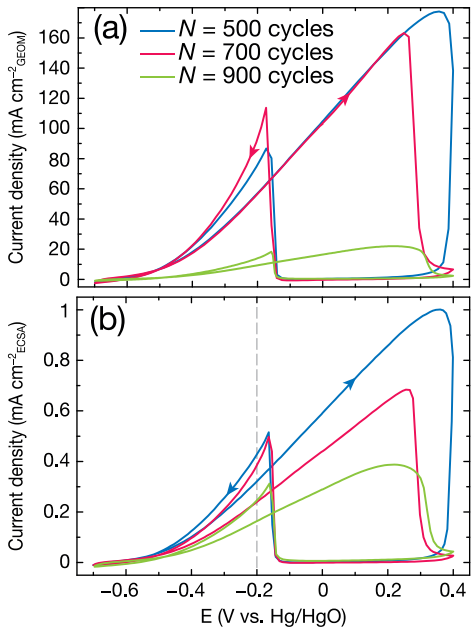

Figure 11. Cyclic voltammograms of Pd/TNTswith various number of Pd ALD cycles on annealed TNTs in 1M KOH + 1M C_2H_5OH . Current density is given per geometrical area (a) and ECSA (b). The scan rate is 25 mV s^{-1}.

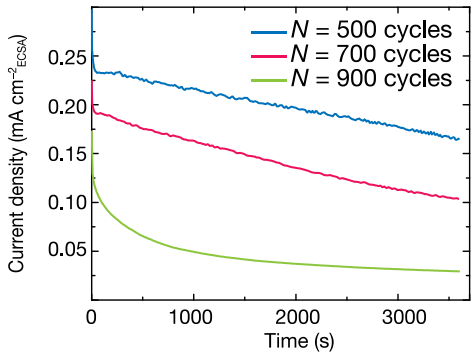

Figure 12. Comparison of the CAs in 1 M KOH + 1 M C_2H_5OH of the different loadings on annealed TNTs at the potential held at 0.2 V vs. Hg/HgO for 1 h.